Earth and Planetary Science Letters 486 (2018) 141–154

Contents lists available at ScienceDirect

Earth and Planetary Science Letters

www.elsevier.com/locate/epsl

Unexpected earthquake hazard revealed by Holocene rupture on the Kenchreai Fault (central Greece): Implications for weak sub-fault shear zones

Alex Copley *, Christoph Grützner [1], Andy Howell [2], James Jackson, Camilla Penney, Sam Wimpenny

COMET, Bullard Labs, Department of Earth Sciences, University of Cambridge, Cambridge, UK

ARTICLE INFO

Article history:
Received 27 November 2017
Received in revised form 15 January 2018
Accepted 18 January 2018
Available online 3 February 2018
Editor: R. Bendick

Keywords:
normal faulting
ductile shear zones

ABSTRACT

High-resolution elevation models, palaeoseismic trenching, and Quaternary dating demonstrate that the Kenchreai Fault in the eastern Gulf of Corinth (Greece) has ruptured in the Holocene. Along with the adjacent Pisia and Heraion Faults (which ruptured in 1981), our results indicate the presence of closely-spaced and parallel normal faults that are simultaneously active, but at different rates. Such a configuration allows us to address one of the major questions in understanding the earthquake cycle, specifically what controls the distribution of interseismic strain accumulation? Our results imply that the interseismic loading and subsequent earthquakes on these faults are governed by weak shear zones in the underlying ductile crust. In addition, the identification of significant earthquake slip on a fault that does not dominate the late Quaternary geomorphology or vertical coastal motions in the region provides an important lesson in earthquake hazard assessment.

1. Introduction

Horizontal extension by normal faulting often results in arrays of fault-bounded blocks that have rotated about horizontal axes as their bounding faults slip (so-called 'domino' or 'bookshelf' faulting) (e.g. Gilbert, 1928; Proffett, 1977; Morton and Black, 1975; Jackson and M^{c}Kenzie, 1983). However, questions remain over what controls whether faults positioned across-strike from each other are active simultaneously or sequentially, and how this may vary between different extensional settings (e.g. Jackson et al., 1982; Dart et al., 1995). Additionally, in cases where the location of dominant slip activity migrates across-strike between faults, it is not known whether this transition is sudden or gradual, or what controls the direction of migration (e.g. Goldsworthy and Jackson, 2001). Addressing these questions will reveal important information about the mechanics and behaviour of faults, and will also highlight whether multiple faults in arrays of parallel structures need to be considered as sources of earthquake hazard. In addition, understanding the behaviour of arrays of faults will allow us to probe the properties of the underlying ductile layer. Specifically, we can address the controversy of whether strain accumulation at faults is governed by flow in a laterally-homogeneous viscoelastic material (e.g. Meade et al., 2013), or whether lateral contrasts in effective viscosity are the dominant control (e.g. Yamasaki et al., 2014). We address these questions by making new observations of Holocene fault slip on the Kenchreai Fault on the south side of the Gulf of Corinth in central Greece.

The Kenchreai Fault bounds the south side of the isthmus between the Gulf of Corinth and the Saronic Gulf (Fig. 1). The northern, hangingwall, side of the fault is occupied by the Corinth Terraces – a series of marine terraces, dating from ~0.5 Ma to the present, that have been uplifted by motion on the Heraion (also known as Xylokastro) and Pisia faults to the north (e.g. Armijo et al., 1996). This northern fault system ruptured in M_w6.7 and 6.4 earthquakes in 1981 (e.g. Jackson et al., 1982). The uplift of the Corinth Terraces relative to the sea-level highstands at which they formed (e.g. Armijo et al., 1996) shows that the Heraion and Pisia faults have been more active over the last ~400 kyr than the Kenchreai and Loutraki Faults, motion on which would produce hangingwall subsidence in the region of the terraces. It is likely that the Kenchreai Fault was the most active fault in the region in the early/mid Pleistocene, because the sediments currently exposed in the cutting of the Corinth Canal (Fig. 1; Collier and Dart, 1991) represent a series of climatically-controlled sea-

* Corresponding author.
E-mail address: acc41@cam.ac.uk (A. Copley).
[1] Pressent address: Friedrich Schiller University Jena, Institute of Geological Sciences, Burgweg 11, 07749 Jena, Germany.
[2] Pressent address: Seequent, Addington, Christchurch, New Zealand.

https://doi.org/10.1016/j.epsl.2018.01.014

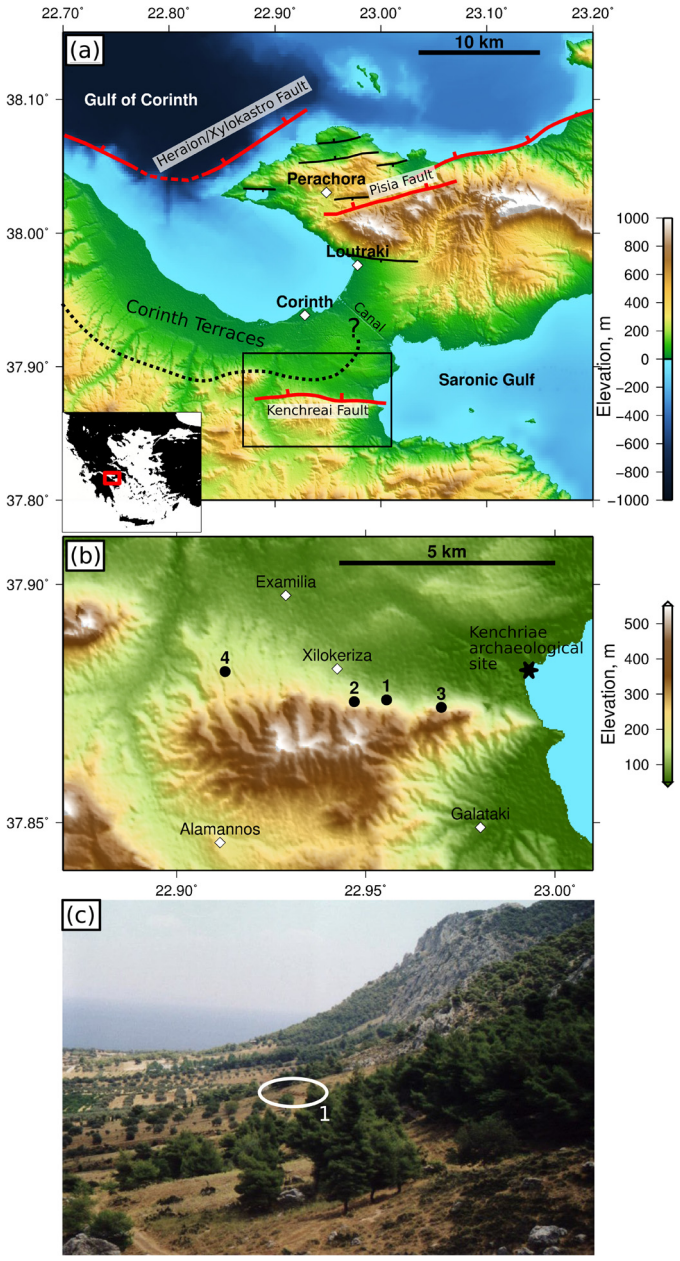

Fig. 1. (a) Overview of the eastern Gulf of Corinth (see inset for location). Red lines show major (~10 km and longer) active faults. Topography is the SRTM 1-arcsecond dataset. The black dotted line shows the approximate extent of the Corinth terraces, which become indistinct where they are affected by the spoil from the Corinth canal. (b) Shows the Kenchreai Fault, in the area outlined by the black box in (a). Our field sites described in the text are labelled 1–4, and our trench is at site 1. (c) View east from site 2, with site 1 visible in the middle-distance, shown by the white circle. (For interpretation of the colours in this figure, the reader is referred to the web version of this article.)

level cycles superimposed upon tectonic subsidence, of which the Kenchreai Fault is thought to be the cause (e.g. Mack et al., 2009; Charalampakis et al., 2014). The rate of activity on the Kenchreai Fault therefore seems to have reduced since the mid Pleistocene, but questions remain as to whether it has been active at all in the latest Quaternary.

Noller et al. (1997) and Goldsworthy and Jackson (2001) described the presence of topographic scarps in alluvial fan surfaces close to the range-front of the Kenchreai Fault, in the locations marked 1 and 2 on Fig. 1b. They interpreted these scarps as having been produced by normal-faulting earthquakes on the Kenchreai Fault. However, there have been suggestions that the scarps may

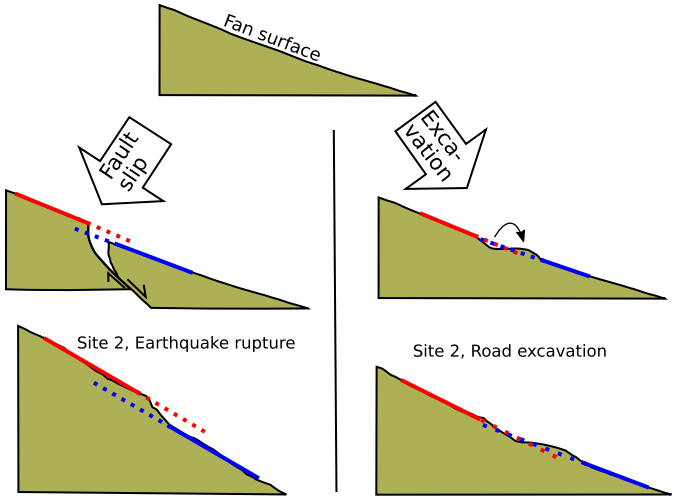

Fig. 2. Examples of the slope morphology formed by earthquake rupture (left) and road excavation or terracing (right) in a fan surface. The lower panels show actual examples of each type of slope morphology from our site 2 on the Kenchreai Fault (Fig. 4d). The earthquake rupture is shown as a shallow tensional fracture in sediments, above the main slip surface, as is often observed in normal-faulting events (e.g. Slemmons, 1957; Jackson and M^{c}Kenzie, 1983). However, the same principles of slope offset apply in the case of a primary fault breaking the surface.

have been formed instead by human excavation, reinforced by the belief that the Kenchreai Fault is now completely inactive (e.g. Mack et al., 2009; Charalampakis et al., 2014). In this paper we survey in detail the scarps described by Noller et al. (1997) and Goldsworthy and Jackson (2001), and two additional newly-discovered scarps also on the Kenchreai Fault. We also describe evidence for palaeoseismicity in a trench we dug across one of the scarps. We then interpret our results from the perspectives of fault and lithosphere rheology, and of earthquake hazard.

2. Tectonic geomorphology

This section presents new high-resolution topographic models of the scarps described by Noller et al. (1997) and Goldsworthy and Jackson (2001), and of two additional sites along the Kenchreai fault where we observe topographic offsets in recent alluvial fan surfaces. We have used topographic profiles at all four sites to assess whether these apparent offsets are anthropogenic (e.g. agricultural terraces, road cuts), or whether they formed in earthquakes. Scarps formed by excavation will be flanked by slopes with different gradients, as a result of the removal of material, but the undisturbed slopes to either side of the excavation will project onto each other (Fig. 2). Earthquake scarps cutting alluvial fans will have a constant slope angle above and below the scarp, and the slopes will not project onto each other across the scarp, representing the offset of a quasi-planar fan surface (Fig. 2). Fan surfaces generally decrease in gradient with distance from the apex (e.g. Whipple and Dunne, 1992; Staley et al., 2006), so in the following discussion we interpret profiles that are short enough (generally tens of metres) that the longer-wavelength curvature of the fans does not affect our offset estimates.

We produced high-resolution digital elevation models (DEMs) at three of the survey sites using the structure-from-motion technique (Westoby et al., 2012; Johnson et al., 2014; Abdrakhmatov et al., 2016). Each site was systematically photographed from ~30–40 m height using a digital camera mounted on a drone. Ground control points distributed across the site were located using differential GPS (dGPS), to a horizontal and vertical accuracy of ~10 cm, to provide a reference frame for the DEM. The photographs were then processed using Agisoft Photoscan to form a dense point cloud with an absolute vertical accuracy of ~20 cm

(but with significantly better relative accuracy between adjacent points), from which all subsequent measurements were made. We also collected topographic profiles across the scarps at all of the sites using dGPS (Campbell et al., 2013; Grützner et al., 2017).

2.1. Site 1

Site 1 (Fig. 1b) corresponds to Fig. 4a in Goldsworthy and Jackson (2001) and was also identified by Noller et al. (1997). The scarp consists of a ~50 m long topographic step trending ENE–WSW, in alluvial fan material ~60 m north of the limestone range front (Fig. 3). The lithology is a mixture of soil and limestone clasts (described in detail in Section 3), and extensive carbonate cementation allows the material to preserve a sub-vertical scarp. DEM and dGPS profiles perpendicular to the scarp indicate 1–1.5 m offset in the fan surface, separating slopes of similar angle above and below, which do not project onto each other if extrapolated across the scarp (Fig. 3c and d). This feature strongly suggests that the scarp is not anthropogenic, and is likely to represent fault slip (Fig. 2). This site is the location of the trench described in Koukouvelas et al. (2017), and our new palaeoseismological trench, which we discuss in Section 3.

2.2. Site 2

Site 2 (Fig. 1b) corresponds to Fig. 4b in Goldsworthy and Jackson (2001) and was also identified by Noller et al. (1997). The scarp is formed in carbonate-cemented scree, and consists of a 100 m long topographic step in a fan surface, down-slope of an area of active agriculture, ~60 m north of the limestone range front (Fig. 4). dGPS profiles across this feature highlight a 0.5–1.0 m vertical offset in the fan surface, with similar slope angles above and below the topographic step that do not project onto each other if extrapolated across the scarp, as expected for an earthquake scarp (Fig. 4c and d). This feature is in contrast to the road cutting further down the slope (50–60 m along the profiles in Fig. 4c and d), which shows dramatically different gradients to either side of the scarp, and is flanked by slopes that do project onto each other if extrapolated across the scarp (see also Fig. 2).

2.3. Site 3

At site 3 (Fig. 1b) we identified a previously undescribed ESE–WNW trending scarp crossing an alluvial fan, which lies directly along-strike from the bedrock-sediment contacts on the margins of the fan (Fig. 5a). Topographic profiles through the aerial DEM across this feature highlight a step in the fan surface (Fig. 5c). However, due to the uneven fan surface and extensive vegetation making photogrammetry- and dGPS-based surveying difficult, these methods are not as reliable as at the sites described above. Instead we used an Abney level to accurately measure the offset in the fan surface. The horizontal locations of survey points were measured by GPS, and the angles between them using the Abney level. Fig. 5d shows a ~0.5 m offset in the fan surface at the location of the scarp.

2.4. Site 4

Site 4 (Fig. 1b) is situated at the western end of the Kenchreai fault. At this locality we identified an offset in an alluvial fan surface ~800 m north of the range front (Fig. 6). In contrast to the scarps described above, this offset occurs over a horizontal distance of 40–60 m, rather than as a single discreet scarp. dGPS profiles across this feature show a ~2 m high surface offset (Fig. 6a). This long-wavelength warping could reflect distributed deformation associated with an earthquake rupture in the poorly consolidated alluvial fan material, or an old and degraded surface rupture that may additionally have been affected by agricultural activity.

2.5. Summary of geomorphology

The four sites described above have topographic profiles consistent with surface ruptures formed in recent earthquakes. The scarps form a discontinuous set along the range-front of the Kenchreai Fault. The individual strikes vary within ~30° of E–W, and the overall strike of the rupture set is ~E–W (Fig. 1b). We saw no evidence of shear surfaces, and the scarps we have described are likely to have been formed by offsets across steeply-dipping tensional fissures, as was observed in many places during the 1981 Gulf of Corinth earthquake sequence (Jackson et al., 1982). The presence of the scarps in the recent sediments, tens to hundreds of metres north of the bedrock-sediment contact at the surface, is consistent with formation by sediments failing in tension above the main slip surface at depth (e.g. Slemmons, 1957; Jackson and M^{c}Kenzie, 1983). By analogy with the 1981 Gulf of Corinth earthquake sequence, the scarp heights we have measured are consistent with one earthquake on a fault with the ~10 km length of the Kenchreai Fault (Jackson et al., 1982), with a magnitude of ~6. If the scarps we have identified are tectonic in origin, we would also expect the stratigraphy in the shallow sub-surface to be offset. In the following section, we present new observations from a palaeoseismological trench that we opened across the scarp at Site 1, to test whether the shallow fan stratigraphy displays evidence for recent surface-rupturing earthquakes.

3. Palaeoseismological trenching

Paleoseismological trenching aims to reconstruct the earthquake history of a fault beyond the available instrumental and historical records (e.g. McCalpin, 2009), and has been applied to a number of normal faults in central Greece (e.g. Pantosti et al., 1996; Collier et al., 1998; Chatzipetros et al., 2005; Grützner et al., 2016).

For the Kenchreai fault, Koukouvelas et al. (2017) opened a 2 m deep trench at site 1 (described above), and reported evidence for four surface rupturing earthquakes in the past 10 ka. However, their trench lies entirely upslope of the morphological step reported in Fig. 4a of Goldsworthy and Jackson (2001) and that we surveyed (Fig. 3). We therefore dug our own trench that actually crosses that scarp.

We opened a 6 m-long trench across the topographic scarp in the fan surface (Fig. 7). The trench exposes typical fan deposits (see Appendix A for details). Layers of fine-to-coarse gravels with occasional blocks of up to 25 cm diameter are either clast-supported or embedded into silty-sandy matrices with varying clay contents. Several units of 5–75 cm thickness can be distinguished based on grain size, sorting, angularity, clay content, and the grade of calcrete cementation. In general, the dip of the layers is sub-parallel to the surface slope, and recent soil covers the units except at the steep scarp. On the western trench wall, within the upslope (footwall) part of the trench, we observe undistorted layers that extend for ~2.5 m from the southern tip of the trench to where they terminate against a ~20 cm wide fissure fill close to the surface scarp. The fissure occurs slightly down-slope of the scarp, presumably indicating ~0.5–1 m of erosion into the scarp since it formed (also suggested by the loose scree casts on the ground down-slope of the scarp; Fig. 3b). To the north of the filled fissure, intact layers can be traced for another 1.5–2 m, before they interfinger with a thick chaotic layer that we interpret as bedding disrupted by ploughing in the adjacent field.

In contrast to the western trench wall, in the eastern wall we found truncated beds (Fig. 7b) rather than a filled fissure. These

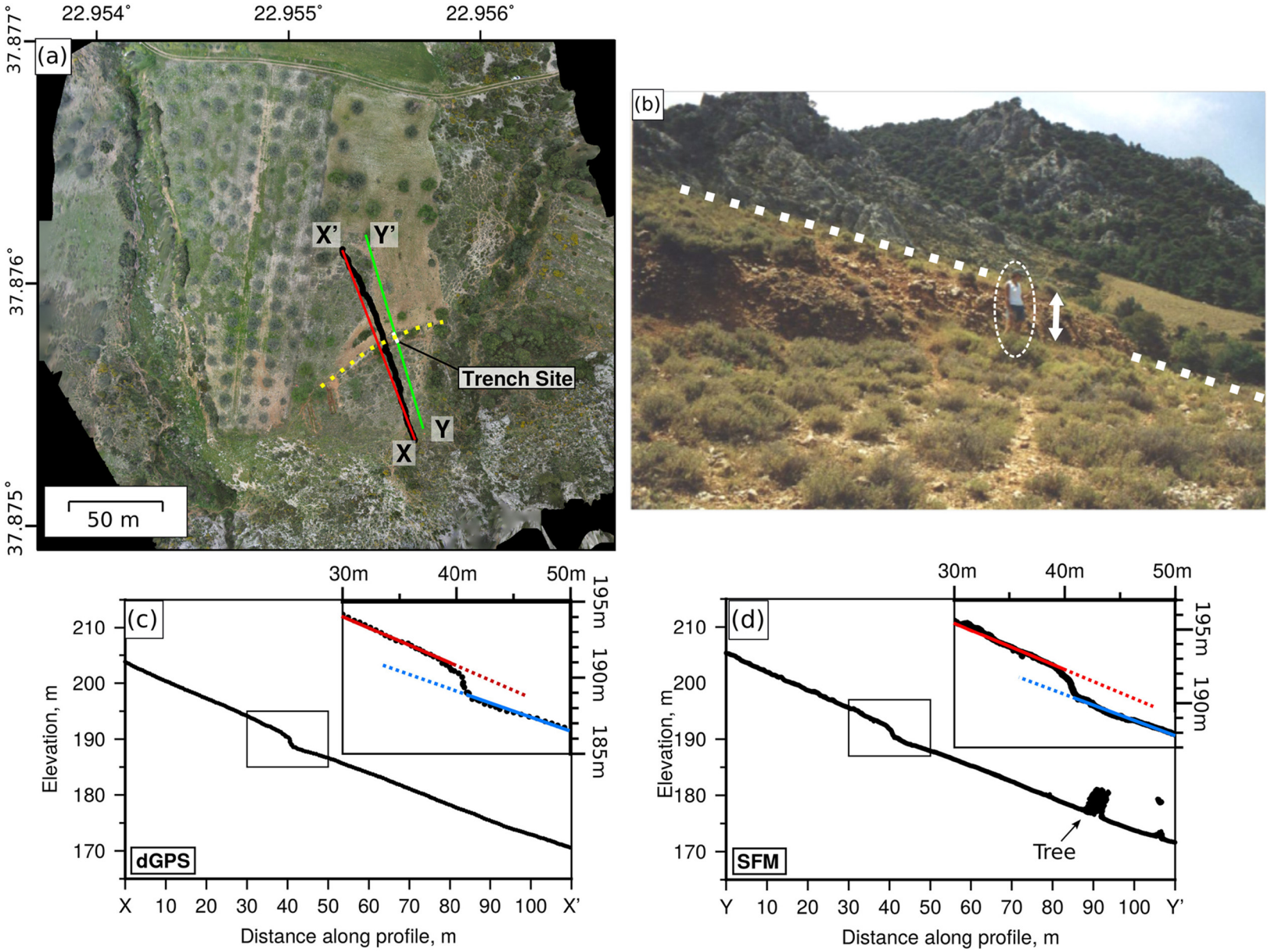

Fig. 3. Measurements at Site 1 (37.876°N, 22.955°E). (a) Shows an orthophoto produced by drone imagery. The white box shows the location of our palaeoseismological trench (Section 3), and the dotted yellow line shows the scarp. dGPS measurement locations are shown in black, and (c) shows these measurements projected onto the red line. Green line shows the location of the profile through the structure-from-motion DEM in (d). (b) Shows the scarp (looking SW), with person circled for scale. (c) dGPS profile, box shows section expanded in inset. (d) Profile through structure-from-motion DEM, box shows section expanded in inset. (For interpretation of the colours in this figure, the reader is referred to the web version of this article.)

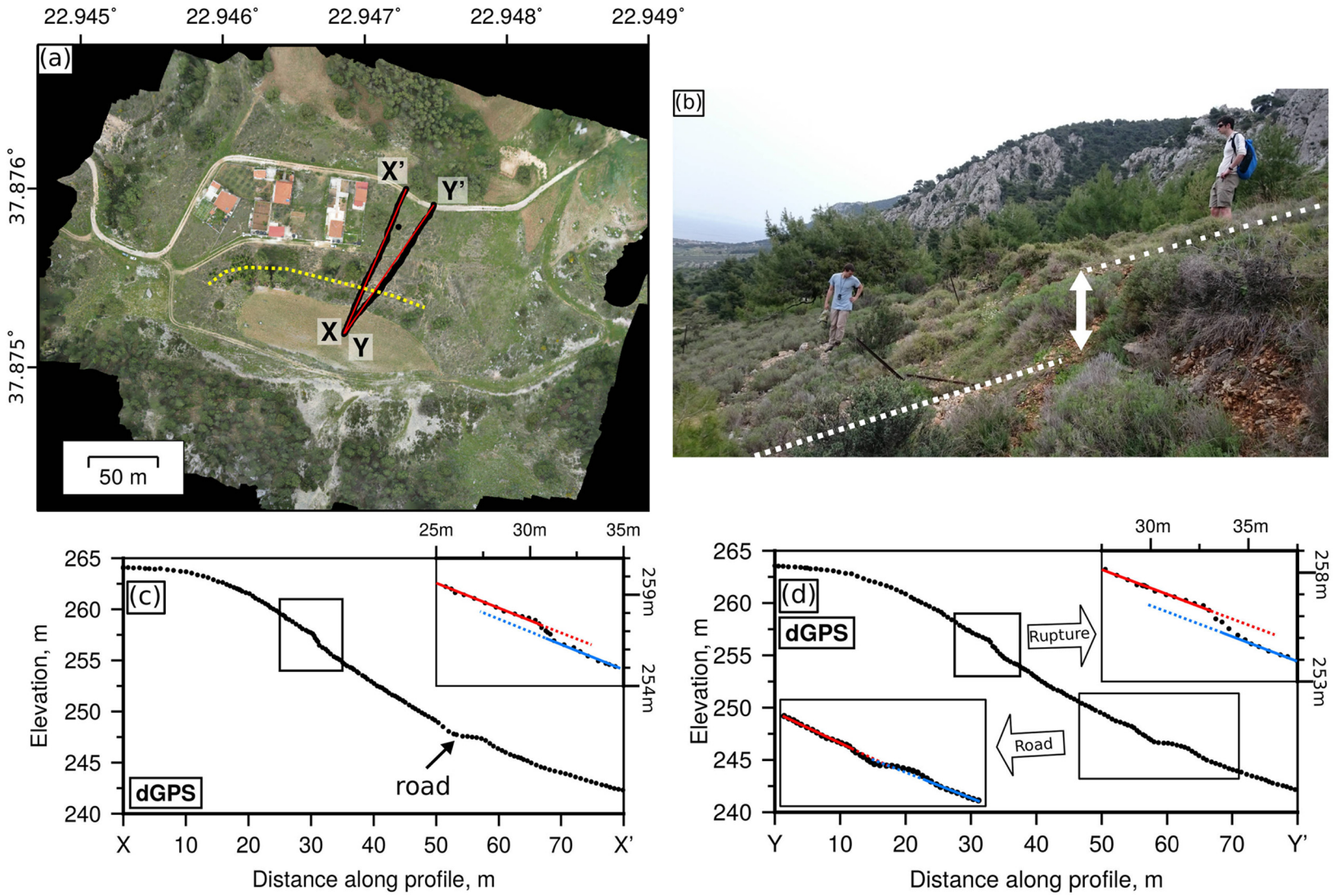

Fig. 4. Measurements at Site 2 (37.875°N, 22.947°E). (a) Shows an orthophoto produced by drone imagery with the locations of dGPS measurements (black lines), which have been projected onto the red lines and shown in (c) and (d). The dotted yellow line shows the location of the scarp. (b) Shows the break in slope, looking ESE. (c) and (d) show dGPS profiles across the scarp, from X–X′ and Y–Y′ respectively. Black boxes shows locations of insets. The data from panel (d) is also shown in Fig. 2. Note that in panel (d) the slopes to either side of the road project onto each other, but those to either side of the scarp we interpret as a fault rupture show an offset. (For interpretation of the colours in this figure, the reader is referred to the web version of this article.)

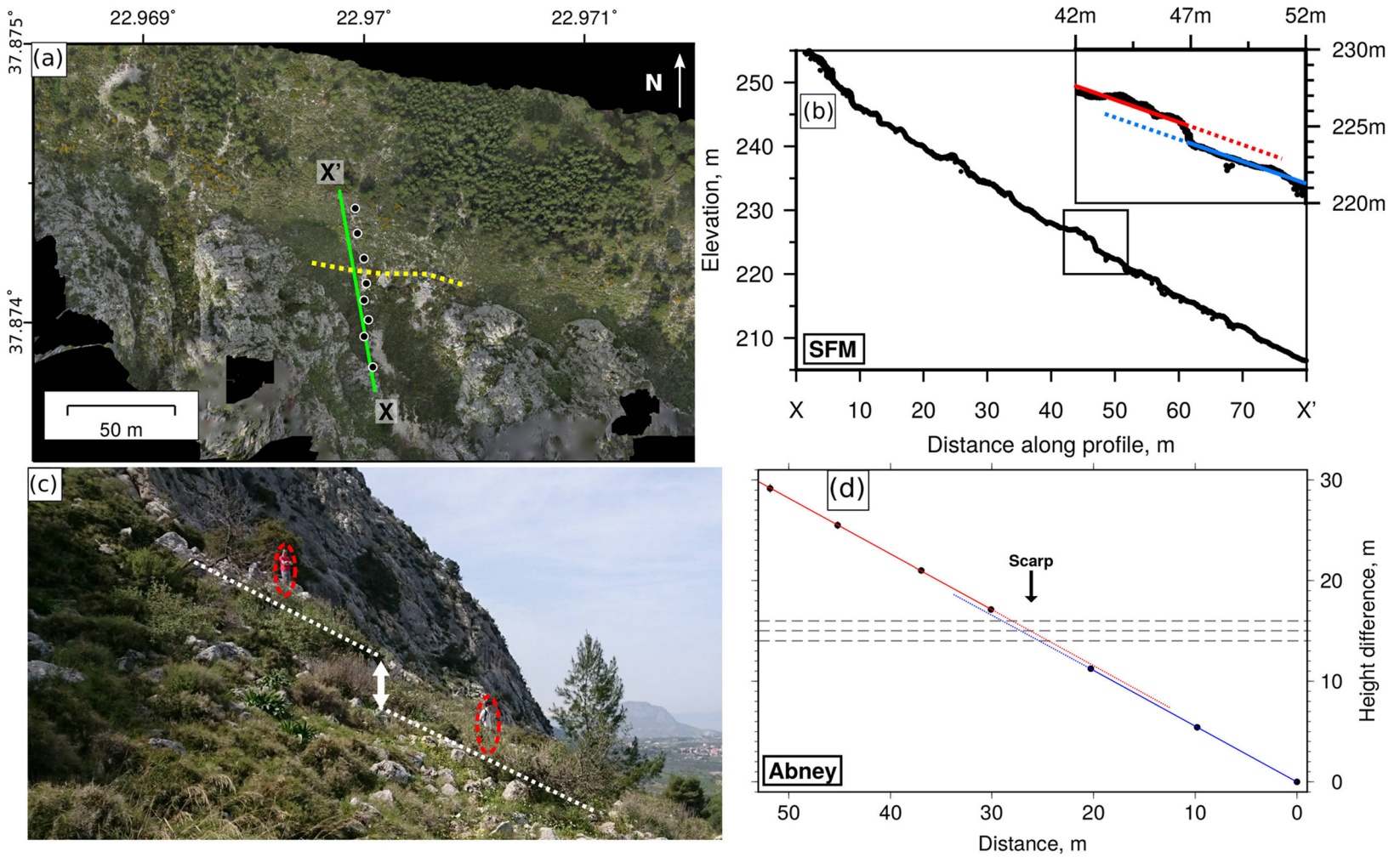

Fig. 5. Measurements at Site 3 (37.874°N, 22.970°E). (a) Shows an orthophoto produced by drone imagery. The green line shows the location of the profile through the DEM in (b), black circles show the locations of the Abney level measurements in (d), and dotted yellow line shows the location of the scarp. (b) Shows a profile through the structure-from-motion DEM. The black box shows the location of the inset. The considerable noise in the DEM is from vegetation coverage. (c) Is a photograph (looking west) of the offset in slope, with people for scale (circled in red). (d) Elevations relative to the northernmost black point in (a), measured using an Abney level. The error bars are smaller than the points, and are a maximum of 0.5 m at the southernmost point (due to propagation of the errors on each measurement), based upon our measurement accuracy of 0.5°. (For interpretation of the colours in this figure, the reader is referred to the web version of this article.)

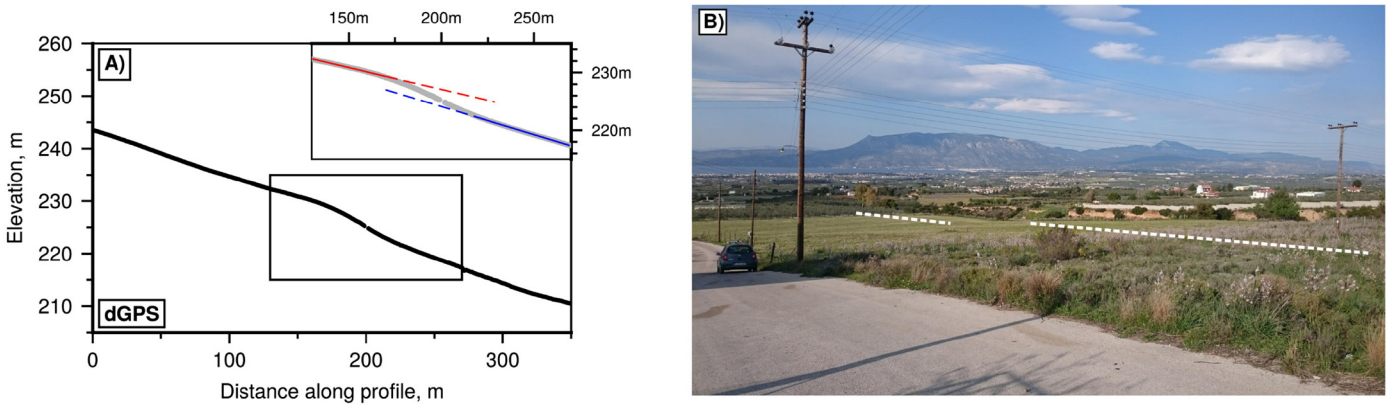

Fig. 6. Measurements at Site 4 (37.882°N, 22.913°E). (a) dGPS profile across the long-wavelength topographic step. Black box shows location of inset. (b) Photo looking northeast showing the slope offset, where the car is parked. The mountain in the background (Gerania) is the uplifted footwall of the Pisia Fault (Fig. 1).

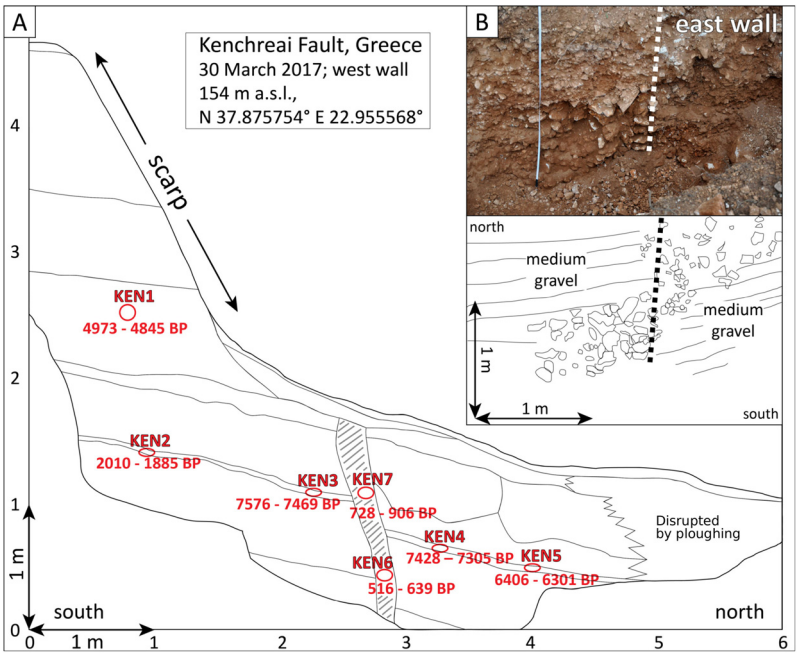

Fig. 7. Paleoseismological trench across the Kenchreai Fault. (A) Sketch of the main units encountered in the west wall of the trench (see Appendix A for a detailed description). In the middle of the trench we observe a filled, almost vertical fissure (grey hatching). Layers are either offset across the fissure or terminate against it, see text for details. Red ellipses mark the location of the bulk radiocarbon samples KEN1–KEN7, ages are reported in years cal BP. Note that the ages are the reported lab results, but that we expect the real uncertainty to be much higher (e.g. ∼1 kyr) because we sampled bulk material. See Appendix B for more details on the samples. Samples KEN2–KEN5 are from slope-parallel, thin clayey layers; samples KEN6, 7 are from the fissure fill; sample KEN1 is from a clay-rich matrix. (B) Detail of the east wall of the trench, showing that instead of a clear fissure we observe layer truncations against a plane (dotted line). No layers can be reliably correlated between footwall and hangingwall. (For interpretation of the colours in this figure, the reader is referred to the web version of this article.)

truncations are in a location along-strike from the fissure seen in the western wall. There are a number of sediment layers that could possibly be correlated across the fault. However, we are unable to estimate an amount of offset that is consistent with all the sediments in both walls of the trench. This observation suggests that the stratigraphy is highly three-dimensional, and that simple sediment correlations parallel to the walls of the trench are inappropriate. However, although we cannot estimate the amount of offset, the filled fissure and truncated beds confirm that the shallow sediments have been offset by fault motion.

We took seven bulk radiocarbon samples from the trench in order to constrain the date of the last surface-rupturing earthquake (Fig. 7a). We took four samples from thin layers with high clay content (two samples from the footwall (KEN2, 3) and two samples from the hanging wall (KEN4, 5)). While sample KEN2 returned an age of ∼2 ka cal BP, the other three samples are ∼6.3–7.5 ka cal BP (Fig. 7a; see Appendix B for sample details). Sample KEN1, with an age of ∼4.9 ka cal BP, comes from a stratigraphically younger layer in the footwall. Two more samples were taken from the fissure fill, the lower of which (KEN6) returned an age of 516–639 yrs cal BP. The upper one (KEN7) shows an age of 728–908 yrs cal BP.

Although the nominal errors in sample ages reported by the lab are relatively small, the actual uncertainties in bulk sediment ages are much greater due to the unknown residence time of the carbon in the soil, overprinting, and reworking processes. Thus, the dating results must not be taken as strict layer ages and we assume a possible error of at least 1 ka for each sample (Grützner et al., 2016). With the exception of KEN2, which we regard as an outlier, all samples are in stratigraphic order. We interpret samples KEN3–5 as pre-earthquake, and samples KEN6 and KEN7, which are resolvably younger and from within the vertical fissure, as post-earthquake. Note that open fissures are often filled by older material from the surface. In general the samples show that sedimentation on the alluvial fan was active until at least 4 ka cal BP, indicating that

fan resurfacing post-dates the end of the last glacial maximum. We conclude that there is evidence for an earthquake less than ~1.5 ka before present.

These findings are different from the palaeo-earthquake conclusions published by Koukouvelas et al. (2017) from their trench site less than 50 m west of ours, probably because ours is the only trench to cross the topographic scarp in the fan surface. However, they also report fissure fill related to an event that happened after 660 AD, which is consistent with our data, and may represent off-fault deformation in the footwall of the fault where their trench is located. Since radiocarbon dating provides only a rough age estimate for the last surface rupturing earthquake, in the next section we discuss historical and archaeological evidence for strong earthquakes in the region.

4. Historical and archaeological record

The Corinthian harbour of Kenchreai is a world-famous archaeological site (Fig. 1b) containing buildings which lie below present-day sea level (Scranton and Ramage, 1967; Flemming, 1993). The proximity to the Corinth terraces on the remainder of the isthmus suggests that, if tectonic, this subsidence may be a transient feature superimposed on longer-term uplift. However, whether or not the submergence is related to earthquake activity, possibly on the Kenchreai Fault, has been widely discussed (e.g. Alexouli-Leivaditi et al., 2008; Koukouvelas et al., 2017). It was stressed by Rothaus et al. (2008) that the archaeological record for tectonic subsidence and destructive earthquakes is limited at best, with submerged fish tanks being the only solid evidence for subsidence between AD 80 and AD 1964 that cannot be explained by Holocene sea-level rise (Lambeck, 1995; Lambeck and Purcell, 2005). However, the predictions of glacial isostatic adjustment models in the eastern Mediterranean are made uncertain by the unknown and probably laterally-variable mantle rheology around the Hellenic subduction zone. Kolaiti and Mourtzas (2016) recently published a new sea level curve for the Western Saronic Gulf and re-interpreted the archaeological evidence of subsidence at Kenchreai. It therefore remains unclear whether the Kenchreai archaeological site records earthquake-related subsidence due to the Kenchreai fault.

Historical reports of earthquakes in the study area are abundant (Papazachos and Papazachou, 1997), but the reliability of old accounts is often hard to assess. Koukouvelas et al. (2017) compiled a review of the available sources. Seismic events in the 1st Century AD that affected Corinth are seemingly well-documented, but the causative faults remain unknown. The sources for most of the later earthquakes that caused damage to Corinth and neighbouring settlements are also uncertain – none of the events mentioned in the literature can be unequivocally assigned to the Kenchreai Fault. The 1858 Corinth Earthquake, which had an estimated magnitude of 6.5, may have had its epicentre close to the Kenchreai Fault and may be recorded in the trench of Koukouvelas et al. (2017). We conclude that archaeological and historical records are consistent with recent ruptures on the Kenchreai Fault, but we are unable to link the scarp and the earthquake evidence from our trench to a specific historical event. This is a common issue, even in Greece with its excellent historical record (see also Grützner et al., 2016). What is unavoidable is that any earthquakes on the Kenchreai Fault would lead to subsidence of the Kenchreai archaeological site, which is positioned in the immediate hangingwall of the fault.

5. Discussion

5.1. Parallel faults and migration of activity

The results of our topographic surveying and palaeoseismic trenching demonstrate that the Kenchreai fault has experienced over 1 m of fault offset during the Holocene. When combined with the magnitude 6 earthquakes that occurred in 1981 on the Heraion and Pisia faults to the north, our observations show that multiple, parallel, normal faults have all been active in the Holocene. These faults dip in the same direction and are closely-spaced (~15–20 km across-strike), in the sense that each will experience significant stress changes due to earthquakes on the other faults.

The overall extension in the eastern Gulf of Corinth is not partitioned equally between the faults. The uplifted Corinth terraces are in the hangingwall of the Kenchreai Fault and the footwall of the Pisia and Heraion Faults. The 15–25 km length-scale of the tilting of these terraces, which is continuous and clear around the western edge of the Corinth Bay itself, shows the uplift to be due to motion on the Pisia and Heraion Faults rather then regional uplift due to sub-lithospheric processes (Armijo et al., 1996). Normal-faulting results in significantly larger hangingwall subsidence than footwall uplift (e.g. Jackson and M^{c}Kenzie, 1983). There must therefore be many fewer earthquakes on the Kenchreai Fault than on the Heraion and Pisia Faults during the past ~0.5 Ma, otherwise the Kenchreai Fault would dominate the vertical motions in the Corinth isthmus, and the region of the uplifted terraces would have subsided. Prior to this time period, it is likely that the Kenchreai Fault was the most active structure in the region (e.g. Mack et al., 2009; Charalampakis et al., 2014), as over 1 km of Pliocene to Pleistocene basin sediments were deposited in the region now occupied by the Corinth Isthmus (e.g. Collier and Dart, 1991), in the hangingwall of the Kenchreai Fault. These observations therefore point to a northwards migration of dominant activity within the fault system. A similar pattern is seen further west along the Gulf of Corinth, where deltas deposited in the subsiding hangingwalls of normal faults on the south side of the gulf are now uplifted above sea level by faults that run close to the current shoreline (e.g. Goldsworthy and Jackson, 2001). However, a crucial new observation that we have made at Kenchreai is that the less active fault, to the south of those that control the present-day vertical motions, is still capable of occasional earthquakes. Swarms of small earthquakes ($M < 4$) on the down-dip extensions of faults that are in the footwalls of the dominant basin-bounding faults in the western Gulf of Corinth (Kapetanidis et al., 2015) may imply that those old and relatively inactive faults (Goldsworthy and Jackson, 2001) are also able to generate occasional large earthquakes.

5.2. Causes of migration of activity

A range of processes may contribute to the across-strike migration of activity within systems of parallel normal faults. Migration may occur when it is energetically more favourable to break a new normal fault rather than to continue to slip on a plane which no longer has an optimum orientation, as rotation during slip lowers the dip (e.g. Proffett, 1977; Collettini and Sibson, 2001). Alternatively, migration may occur when the gravitational potential energy contrast across the fault (between uplifted bedrock footwalls and downthrown sediments and water) is sufficient that it is more energetically favourable to break a new fault than to continue increasing the potential energy contrast across the existing structure (e.g. Jackson and White, 1989; Foster and Nimmo, 1996). The cause of migration in another model is when the degree of bending to either side of a fault produces elastic stresses that balance the tractions on the fault plane, limiting further slip (e.g. Scholz and Contreras, 1998). Taken in isolation, all of these explanations suggest that when a new fault has formed, slip on it should be more energetically favourable than on the older structure, and the migration of activity onto the new fault should be instantaneous and complete. However, such a view is inconsistent with our observations of recent activity at Kenchreai, and suggests that additional processes are operating.

5.3. Rheology of the ductile lower crust

The models of fault migration described above can be consistent with our observations from Kenchreai if the behaviour of the ductile region below the seismogenic layer is also considered. It is possible for slip to occur on multiple faults with differing failure stresses if the locations and rates of fault loading are controlled by the deformation in the ductile lower crust, beneath the faults. In this case, faults that are no longer the weakest component of a system, and which require greater applied stresses to slip than do the presently-dominant structures, can still be active if they are loaded to sufficient levels by ductile deformation at depth. Our observations therefore relate to the ongoing debate regarding the geometry and causes of fault loading by deformation in the ductile part of the lithosphere (e.g. Sibson, 1977; Hetland and Hager, 2005; Burgmann and Dresen, 2008; Meade et al., 2013; Yamasaki et al., 2014; Ingleby and Wright, 2017). Geodetic observations have imaged rapid postseismic transient motions, and also interseismic strain which is concentrated around fault zones. Two models have been proposed to explain both of these phenomena. In the first, the ductile lithosphere has a laterally-heterogeneous viscosity, for example due to grain-size reduction and fabric development in shear zones beneath faults (e.g. Sibson, 1977; Burgmann and Dresen, 2008). In this case the rapid postseismic deformation represents the relaxation of both the shear zone and the ambient lithosphere, and interseismic deformation is concentrated near the fault because the deformation in the lower lithosphere (to which the elastic upper crust is coupled) is concentrated in the weak sub-fault shear zone (Fig. 8a). Yamasaki et al. (2014) successfully applied this style of model to the North Anatolian Fault, using observations from before and after the 1999 Izmit and Duzce earthquakes, and Ingleby and Wright (2017) suggested the presence of viscous or frictional shear zones beneath continental faults based upon the rate of decay of transient postseismic motions. A second class of models treats the ductile lithosphere as laterally homogeneous. In this case, a viscoelastic rheology with two or more relaxation timescales is required in order to produce both rapid postseismic transients and also interseismic strain focused around the location of the previous earthquake (e.g. Hetland and Hager, 2005) (Fig. 8b). Meade et al. (2013) demonstrated that this type of model successfully reproduces a catalogue of geodetic observations from strike-slip faults, when a Burgers (bi-viscous) rheology is used for the ductile lithosphere. Our ability to distinguish between these competing models based upon currently available surface geodetic observations is therefore limited, with both classes of models able to fit the data.

The two classes of models described above have largely focused on strike-slip faults with high slip rates and little or no tectonic activity in the immediate surroundings. Our observations of normal-faulting at Kenchreai therefore provide a distinct tectonic situation in which to test these models of lithosphere rheology. In the case that the faults are underlain by weak viscous shear zones, the extension imposed upon the region by far-field tectonic forces will result in extensional strains focused in all shear zones that are weaker than the ambient lower crust, and so will load the overlying faults. It is therefore possible for faults such as Kenchreai to slip, possibly at higher stresses than the Heraion and Pisia faults, because they have experienced interseismic loading by deformation in underlying viscous shear zones (Fig. 8a). For the case where stresses relating to the previous seismic event affect the location of strain accumulation, we need to consider how this mechanism would operate on parallel faults with differing slip rates and earthquake recurrence intervals. The down-dip end of the Kenchreai Fault is beneath the upper parts of the Heraion and Pisia Faults, assuming the seismogenic thickness is ∼15 km (based upon local seismic data (e.g. Hatzfeld et al., 2000)), and assuming a dip of ∼40–50° (which encompasses the majority of active normal faults (e.g. Collettini and Sibson, 2001)). This geometry means that the region down-dip of the Kenchreai Fault will experience stress changes due to earthquakes on both structures. Because the long-term slip rates on the Heraion and Pisia faults are considerably higher than at Kenchreai, during the interseismic period of the Kenchreai Fault the lithosphere immediately down-dip of the fault will experience multiple stress perturbations due to slip on the Heraion and Pisia Faults, and these will come to dominate the stress state (Appendix C). The geometry of deviatoric stresses, and the subsequent motions in the case of a laterally homogeneous Burgers lower crust, will therefore not lead to focused strain beneath the Kenchreai Fault and loading of the upper crust. Our observations from Kenchreai are therefore most consistent with the geometry of interseismic strain accumulation at active faults being due to focused deformation in weak shear zones beneath the faults (Fig. 8a). However, questions remain as to whether this result is globally applicable, and we are not able to use our observations to estimate the width of these shear zones.

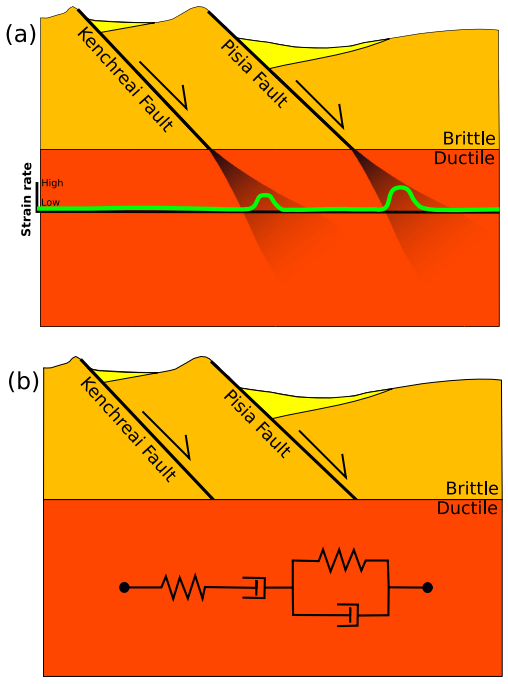

Fig. 8. Possible models of the ductile deformation beneath the Kenchreai and Pisia Faults, as either (a) focused strain in weak shear zones, or (b) flow in a laterally-homogeneous Burgers (bi-viscous) viscoelastic material. The jagged lines represent elastic elements of the viscoelastic material (springs), and the dashpots represent viscous elements.

5.4. Earthquake hazard

The Holocene earthquake rupture on the Kenchreai Fault represents an important lesson in earthquake hazard assessment. The patterns of vertical motion visible at the coast, and the 1981 earthquake sequence on the Pisia and Heraion Faults, lead to the conclusion that most earthquakes in the region happen on these faults. However, our results show that the Kenchreai Fault is capable of producing occasional earthquakes of similar size to those on the more active faults, even though it does not dominate the local geomorphology. Recent thrust-faulting earthquakes have also demonstrated that structures within mountain ranges, away from the obvious range-bounding structures, can break in destructive earthquakes (e.g. Talebian et al., 2006). These results all indicate the need to consider more than just the most geomorphologically obvious faults in a region when assessing earthquake hazard. Al-

though the Kenchreai Fault is clearly less active than others in the region, such faults should be considered when major, long-lived, or hazardous infrastructure projects are being planned.

6. Conclusions

High-resolution elevation models and a palaeoseismic trench demonstrate that the Kenchreai Fault has been active in the Holocene. The presence of parallel, simultaneously active, and closely spaced normal faults indicates that the strain accumulation on the faults is likely to be governed by the existence of weak shear zones in the underlying ductile crust. Faults that appear subservient or inactive in the geomorphology can represent significant sources of earthquake hazard.

Acknowledgements

The authors contributed equally to this work, and are listed in alphabetical order. We thank Richard Rothaus for insights into the archaeology of Kenchreai, and two anonymous reviewers for comments on the manuscript. This work forms part of the NERC- and ESRC-funded project 'Earthquakes Without Frontiers', and was partly funded by the NERC grant 'Looking Inside the Continents from Space'.

Appendix A. Trench description

This appendix documents in detail the units encountered in the paleoseismological trench (Figs. A.1 and A.2) at the Kenchreai Fault (N37.87574 E22.95556, 154 m asl). We distinguish a footwall (southern part) and a hanging wall (northern part) based on the occurrence of a filled vertical fissure. Sedimentological units are offset across the fissure or terminate against it. We labelled the units from the trench floor to the top, beginning in the footwall (units 1–9) with unit 9 marking the recent soil. Units 10–17 are layers found in the hanging wall. Unit 18 is the fissure fill; unit 19 represents colluvium covering the fissure. The hanging wall and unit 19 are also covered by the recent soil (unit 9).

Unit 1

- Clast-supported coarse limestone gravels with clasts of up to 10 cm diameter; subangular-angular; relatively well sorted;
- Silty-fine sandy matrix with little clay, dark brown;
- No layering; not cemented; top of unit dipping to the N; base of unit not visible

Unit 2

- Matrix-supported fine-medium limestone gravels; rounded-subrounded; well sorted;
- Reddish–brownish silty-sandy matrix with little clay;
- Not cemented; very loose; top of unit dipping ∼15° to the N; concordant contact to unit 1

Unit 3

- Thin (∼5–10 cm) matrix-supported layer with few fine-medium limestone gravels; rounded; poorly sorted;
- Reddish–brownish silty matrix with relatively high clay content; rather humid;
- Not cemented; sticky; compact; concordant contact to unit 2; probably representing a period of stable conditions and soil formation;
- A bulk radiocarbon sample from the southern part of this unit, KEN2, returned an age of 2010–1885 cal BP;
- A bulk radiocarbon sample from the northern part of this unit, KEN3, returned an age of 7576–7469 cal BP

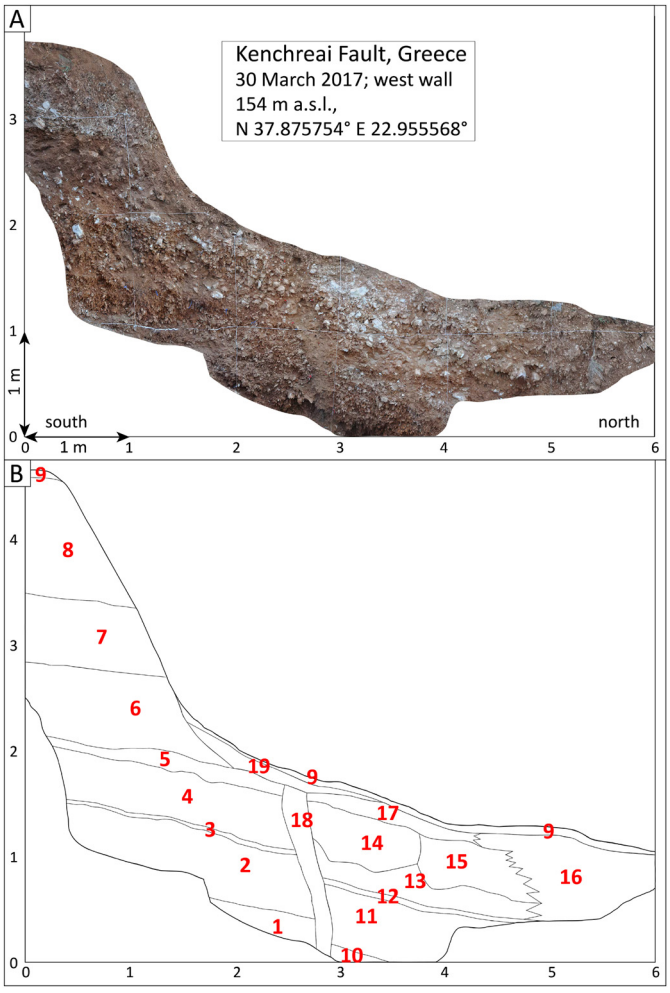

Fig. A.1. Upper panel: Orthophoto of the west wall of the trench at the Kenchreai Fault, stitched from several photos (Nikon D90 SLR, 35 mm lens) using the Structure-from-Motion photogrammetry software Agisoft Photoscan. The line grid nodes (1 × 1 m) were used as control points. Note that the uppermost part of the trench is missing in the orthophoto, but has been sketched in detail. Lower panel: Trench log with the unit numbers described in the text.

Unit 4

- Medium-coarse limestone gravels with clast of up to 20 cm diameter; poorly sorted; subangular-angular; matrix-supported at the base, increasingly clast-supported to the top without any sharp transition
- Silty-sandy matrix; little clay, reddish at the base, whitening to the top;
- No layering; loose at the base, increasingly cemented to the top; concordant contact to unit 3

Unit 5

- Matrix-supported fine-coarse limestone gravels; poorly sorted; subangular to rounded;
- Well cemented; $CaCO_3$ precipitated, compact calcrete layer; white; concordant contact to unit 4

Unit 6

- Matrix-supported mainly coarse limestone gravels with clasts of up to 15 cm diameter; well sorted; subangular;
- Reddish–brownish silty-sandy matrix with intermediate clay content;
- Not cemented, rather compact, sticky; concordant contact to unit 5;

Fig. A.2. Orthophoto of the west wall of the trench.

– A bulk radiocarbon sample from the top of this unit, KEN1, returned an age of 4973–4845 cal BP.

Unit 7

– Clast-supported medium-coarse limestone gravels with clasts of up to 10 cm diameter; bimodal last grain size distribution; subangular;
– Silty-fine sandy matrix; light grey to white
– Somewhat cemented by $CaCO_3$; concordant to unit 6

Unit 8

– Matrix-supported mainly coarse limestone gravels with clasts of up to 20 cm diameter; poorly sorted; subangular;
– Reddish–brownish silty-sandy matrix with intermediate clay content;
– Not cemented, rather loose, concordant contact to unit 7

Unit 9

- Recent soil

Unit 10

- Clast-supported coarse limestone gravels with clasts of up to 10 cm diameter; subangular-angular; relatively well sorted;
- Silty-fine sandy matrix with little clay, dark brown;
- No layering; not cemented; top of unit dipping to the N; base of unit not visible

Unit 11

- Matrix-supported fine-medium limestone gravels; rounded-subrounded; well sorted;
- Reddish–brownish silty-sandy matrix with little clay;
- Not cemented; very loose; top of unit dipping ∼15° to the N; concordant contact to unit 10

Unit 12

- Thin (∼5–10 cm) matrix-supported layer with few fine-medium limestone gravels; rounded; poorly sorted;
- Reddish–brownish silty matrix with relatively high clay content; rather humid;
- Not cemented; sticky; compact; concordant contact to unit 11; probably representing a period of stable conditions and soil formation; similar to unit 3 in the footwall;
- A bulk radiocarbon sample from the southern part of this unit, KEN4, returned an age of 7428–7305 cal BP;
- A bulk radiocarbon sample from the northern part of this unit, KEN5, returned an age of 6406–6301 cal BP

Unit 13

- Matrix-supported medium-coarse limestone gravels with clast of up to 10 cm diameter; poorly sorted; subangular–angular;
- Silty-sandy matrix; little clay, reddish at the base, whitening to the top;
- No layering; loose; concordant contact to unit 12; interfingering with unit 16 to the north

Unit 14

- Clast-supported medium-coarse limestone gravels with clast of up to 25 cm diameter; poorly sorted; subangular–angular;
- Silty-fine sandy matrix; light grey to white
- Well-cemented; large pores and large pore volume; no layering; concordant contact to unit 13; adjacent to unit 15 to the north

Unit 15

- Clast-supported coarse limestone gravels with clast of up to 15 cm diameter; poorly sorted; subangular-angular;
- Silty-sandy matrix with moderate clay content; greyish-brown;
- Not cemented; no layering; concordant contact to unit 13; adjacent to unit 14 to the south; interfingering with unit 16 to the north

Unit 16

- Matrix-supported fine-coarse limestone gravels with few large clasts; poorly sorted; partly rounded;
- Silty-coarse sandy matrix, poorly sorted, low clay content; greyish-brown;
- Chaotic texture; no layering; not cemented; loose material; probably reworked by ploughing and other farming activities

Unit 17

- Matrix-supported fine-coarse limestone gravels; poorly sorted; subangular to rounded;
- Well cemented; $CaCO_3$ precipitated, compact calcrete layer; greyish–whitish; concordant contact to units 14 and 15; similar to unit 5

Unit 18

- Steeply north dipping unit interpreted as the infill of a subvertical fissure;
- Matrix-supported, few fine-coarse limestone gravels; poorly sorted; rounded to subangular; clast size increase to the top
- Clayey-silty matrix, greyish-brownish at the base, reddening towards the top;
- No layering; no clast imbrication or alignment; chaotic texture; covered by unit 19;
- A bulk radiocarbon sample from the lower part of this unit, KEN6, returned an age of 516–639 cal BP;
- A bulk radiocarbon sample from the upper part of this unit, KEN7, returned an age of 728–906 cal BP

Unit 19

- Matrix-supported, medium-coarse limestone gravels; poorly sorted, subangular to rounded;
- Reddish–light brownish silty matrix; low-moderate clay content;
- Not cemented; no layering; loose material;
- This units is the most recent colluvium from the scarp, capping all other units and overlain only by the recent soil

Appendix B. Sample dating results

Radiocarbon dating results (see Table B.1) of the seven samples collected from the trench. Dating was done by BETA Analytic (Miami, FL, USA) and INTCAL13 was used for calibration (Reimer et al., 2013, Int-Cal13 and Marine13 radiocarbon age calibration curves 0–50,000 years cal BP. Radiocarbon, 55 (4), 1869–1887).

Appendix C. Stress calculations

This appendix shows some calculations for the deviatoric stresses in the ductile layer following earthquakes on parallel normal faults in the brittle upper crust. We calculate the stress changes from slip on elastic dislocations, using the method of Okada (1992). We use normal faults dipping at 45°, and choose the thickness of the brittle layer and the spacing between the faults to be 15 km, in order to replicate the Kenchreai and Pisia Faults. Our results are shown in Fig. C.1. Panel (a) shows the results from an earthquake on the Kenchreai Fault (lefthand fault), and panel (b) shows the addition of three earthquakes on the Pisia Fault (righthand fault). Note that we have not modelled the relaxation in the ductile layer, which is beyond the scope of this study. However, the un-relaxed situation we have shown is equivalent to the maximum importance the stresses from the earthquake on the Kenchreai Fault can have – relaxation would reduce these stress changes in the time interval between that earthquake and those on the Pisia Fault. Panel (b) shows that the stress changes from

Table B.1
Radiocarbon dating results. See Fig. 7 for sample locations.

Sample	Lab code	Material and pre-treatment	d13C	Conventional age	2-sigma calibration	D14C
KEN1	Beta463522	organic sediment, acid washes	−23.6	4340 ± 30 BP	Cal BC 3024–2896 (95.4 %) (Cal BP 4973–4845)	−417.41 ± 21.8‰
KEN2	Beta463523	organic sediment, acid washes	−23.8	2010 ± 30 BP	Cal BC 61–Cal AD 65 (91.2 %) (Cal BP 2010–1885)	−221.37 ± 2.91‰
KEN3	Beta463524	organic sediment, acid washes	−23.4	6640 ± 30 BP	Cal BC 5627–5520 (95.4 %) (Cal BP 7576–7469)	−562.46 ± 1.63‰
KEN4	Beta463525	organic sediment, acid washes	−23.4	6440 ± 30 BP	Cal BC 5479–5356 (94.6 %) (Cal BP 7428–7305)	−551.43 ± 1.68‰
KEN5	Beta463526	organic sediment, acid washes	−23.4	5570 ± 30 BP	Cal BC 4457–4352 (95.4 %) (Cal BP 6406–6301)	−500.12 ± 1.87‰
KEN6	Beta463527	organic sediment, acid washes	−24.6	550 ± 30 BP	Cal BC 1386–1434 (54.9 %) *or* 1311–1359 (40.5 %) (Cal BP 564–516 *or* 639–591)	−66.18 ± 3.49‰
KEN7	Beta463528	organic sediment, acid washes	−24.4	880 ± 30 BP	Cal BC 1117–1222 (68.4 %) *or* 1042–1104 (27.0 %) (Cal BP 833–728 *or* 908–846)	−103.76 ± 3.35‰

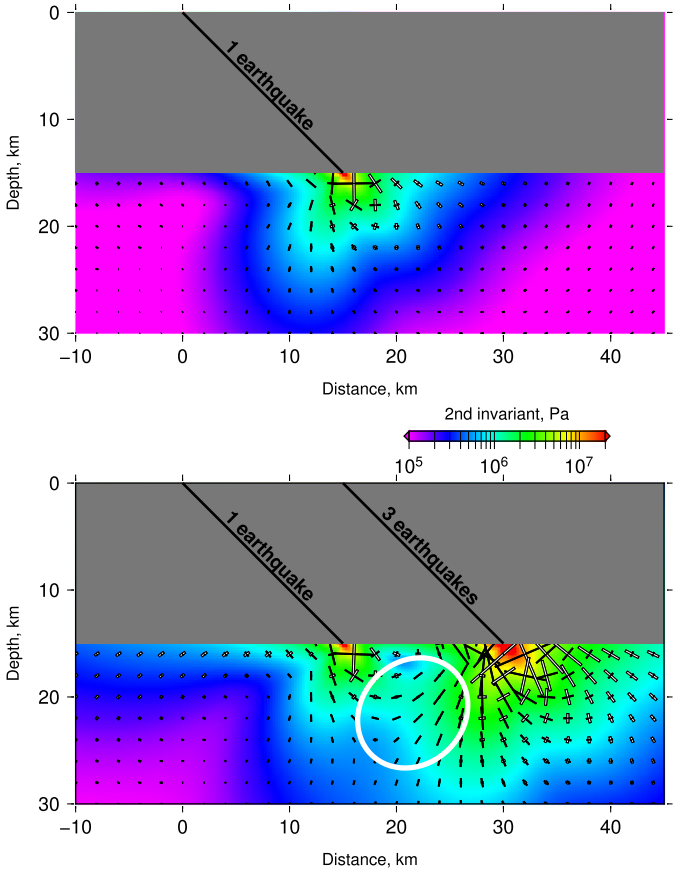

Fig. C.1. Stress changes due to motion on two parallel and closely-spaced normal faults. The grey layer represents the brittle upper crust. The bars show the principal axes of the deviatoric stress tensor. The white bars show compressional stresses and the black bars show extensional stresses. The colour-shading shows the magnitude of the second invariant of the deviatoric stress tensor. The values scale linearly with the amount of slip on the faults, here modelled as 1.5 m in each earthquake. The white circle shows the region down-dip of the lefthand fault that is discussed in the text.

events on the Pisia fault rapidly come to dominate the stress state in the majority of the ductile crust down-dip from the Kenchreai fault (white circle on Fig. C.1), with the exception of a small area at the fault tip. Motion in response to these stresses would not lead to loading of the Kenchreai fault.

References

Abdrakhmatov, K.E., Walker, R.T., Campbell, G.E., Carr, A.S., Elliott, A., Hillemann, C., Hollingsworth, J., Landgraf, A., Mackenzie, D., Mukambayev, A., Rizza, M., Sloan, R.A., 2016. Multisegment rupture in the 11 July 1889 Chilik earthquake (Mw 8.0–8.3), Kazakh Tien Shan, interpreted from remote sensing, field survey, and paleoseismic trenching. J. Geophys. Res. 121, 4615–4640. https://doi.org/10.1002/2015JB012763.

Alexouli-Leivaditi, A., Poulos, S.E., Leivaditis, G., Andris, P.D., Pomoni, F., 2008. An investigation of natural processes and human impact in the coastal area surrounding the ancient harbour of Kenchreai (Saronikos Gulf). Bull. Geol. Soc. Greece 42, 1–6.

Armijo, R., Meyer, B., King, G.C.P., Rigo, A., Papanastassiou, D., 1996. Quaternary evolution of the Corinth Rift and its implications for the Late Cenozoic evolution of the Aegean. Geophys. J. Int. 126, 11–53.

Burgmann, R., Dresen, G., 2008. Rheology of the lower crust and upper mantle: evidence from rock mechanics, geodesy, and field observations. Annu. Rev. Earth Planet. Sci. 36, 531–567.

Campbell, G.E., Walker, R.T., Abdrakhmatov, K., Schwenninger, Jl., Jackson, J., Elliott, J.R., Copley, A., 2013. The Dzhungarian fault: Late Quaternary tectonics and slip rate of a major right-lateral strike-slip fault in the northern Tien Shan region. J. Geophys. Res. 118, 5681–5698. https://doi.org/10.1002/jgrb.50367.

Charalampakis, M., Lykousis, V., Sakellariou, D., Papatheodorou, G., Ferentinos, G., 2014. The tectono-sedimentary evolution of the Lechaion Gulf, the south eastern branch of the Corinth graben, Greece. Mar. Geol. 351, 58–75.

Chatzipetros, A., Kokkalas, S., Pavlides, S., Koukouvelas, I., 2005. Palaeoseismic data and their implication for active deformation in Greece. J. Geodyn. 40, 170–188.

Collettini, C., Sibson, R.H., 2001. Normal faults, normal friction? Geology 29, 927–930.

Collier, R.E., Pantosti, D., D'addezio, G., De Martini, P.M., Masana, E., Sakellariou, D., 1998. Paleoseismicity of the 1981 Corinth earthquake fault: seismic contribution to extensional strain in central Greece and implications for seismic hazard. J. Geophys. Res. 103, 30,001–30,019.

Collier, R.E.L., Dart, C.J., 1991. Neogene to Quaternary rifting, sedimentation and uplift in the Corinth Basin, Greece. J. Geol. Soc. Lond. 148, 1049–1065.

Dart, C., Cohen, H.A., Akyuz, H.S., Barka, A., 1995. Basinward migration of riftborder faults: implications for facies distributions and preservation potential. Geology 23, 69–72.

Flemming, N.C., 1993. Predications of relative coastal sea-level change in the Mediterranean based on archaeological, historical, and tide-guage data. In: Jeftic, L., Milliman, J.D., Sestini, G. (Eds.), Climatic Change and the Mediterranean. Edward Arnold, London.

Foster, A., Nimmo, F., 1996. Comparisons between the rift systems of East Africa, Earth and Beta Regio, Venus. Earth Planet. Sci. Lett. 143, 183–195.

Gilbert, G.K., 1928. Studies of Basin-Range Structure. USGS professional paper No. 153.

Goldsworthy, M., Jackson, J., 2001. Migration of activity within normal fault systems: examples from the Quaternary of mainland Greece. J. Struct. Geol. 23, 489–506.

Grützner, C., Schneiderwind, S., Papanikolaou, I., Deligiannakis, G., Pallikarakis, A., Reicherter, K., 2016. New constraints on extensional tectonics and seismic hazard in northern Attica, Greece: the case of the Milesi Fault. Geophys. J. Int. 204, 180–199.

Grützner, C., Carson, E., Walker, R.T., Rhodes, E.J., Mukambayev, A., Mackenzie, D., Elliott, J.R., Campbell, G., Abdrakhmatov, K., 2017. Assessing the activity of faults in continental interiors: palaeoseismic insights from SE Kazakhstan. Earth Planet. Sci. Lett. 459, 93–104.

Hatzfeld, D., Karakostas, V., Ziazia, M., Kassaras, I., Papadimitriou, E., Makropoulos, K., Voulgaris, N., Papaioannou, C., 2000. Microsesmicity and faulting geometry in the Gulf of Corinth (Greece). Geophys. J. Int. 141, 438–456.

Hetland, E.A., Hager, B.H., 2005. Postseismic and interseismic displacements near a strike-slip fault: a two-dimensional theory for general linear viscoelastic rheologies. J. Geophys. Res. 110. https://doi.org/10.1029/2005JB003689.

Ingleby, T., Wright, T.J., 2017. Omori-like decay of postseismic velocities following continental earthquakes. Geophys. Res. Lett. 44, 3119–3130.

Jackson, J.A., White, N.J., 1989. Normal faulting in the upper continental crust: observations from regions of active extension. J. Struct. Geol. 11, 15–36.

Jackson, J.A., Gagnepain, J., Houseman, G., King, G.C.P., Papadimitriou, P., Soufleris, C., Virieux, J., 1982. Seismicity, normal faulting, and the geomorphological development of the Gulf of Corinth (Greece): the Corinth earthquakes of February and March 1981. Earth Planet. Sci. Lett. 57, 377–397.

Jackson, J.A., M^{c}Kenzie, D., 1983. The geometrical evolution of normal fault systems. J. Struct. Geol. 5, 471–482.

Johnson, K., Nissen, E., Saripalli, S., Arrowsmith, R., McGarey, P., Scharer, K., Williams, P., Blisniuk, K., 2014. Rapid mapping of ultrafine fault zone topography with structure from motion. Geosphere 10 (5). https://doi.org/10.1130/GES01017.1.

Kapetanidis, V., Deschamps, A., Papadimitriou, P., Matrullo, E., Karakonstantis, A., Bozionelos, G., Kaviris, G., Serpetsidaki, A., Lyon-Caen, H., Voulgaris, N., Bernard, P., Sokos, E., Makropoulos, K., 2015. The 2013 earthquake swarm in Helike, Greece: seismic activity at the root of old normal faults. Geophys. J. Int. 202, 2044–2073.

Kolaiti, E., Mourtzas, N., 2016. Upper Holocene sea level changes in the west Saronic Gulf, Greece. Quat. Int. 401, 71–90.

Koukouvelas, I.K., Zygouri, V., Papadopoulos, G.A., Verroios, S., 2017. Holocene record of slip-predictable earthquakes on the Kenchreai Fault, Gulf of Corinth, Greece. J. Struct. Geol. 94, 258–274.

Lambeck, K., 1995. Late Pleistocene and Holocene sea-level change in Greece and south-western Turkey: a separation of eustatic, isostatic and tectonic contributions. Geophys. J. Int. 122, 1022–1044.

Lambeck, K., Purcell, A., 2005. Sea level change in the Mediterranean Sea since LGM: model predictions for tectonically stable areas. Quat. Sci. Rev. 24, 1969–1988.

Mack, G.H., Leeder, M.R., Perez-Arlucea, M., 2009. Late Neogene rift-basin evolution and its relation to normal fault history and climate change along the southwestern margin of the Gerania Range, central Greece. Geol. Soc. Am. Bull. 121, 907–918.

McCalpin, J.P., 2009. Palaeoseismology, 2nd edition. Academic Press.

Meade, B.J., Klinger, Y., Hetland, E.A., 2013. Inference of multiple earthquake-cycle relaxation timescales from irregular geodetic sampling of interseismic deformation. Bull. Seismol. Soc. Am. 103, 2824–2835.

Morton, W.H., Black, R., 1975. Crustal attenuation in afar. In: Afar Depression of Ethiopia. Inter-Union Commission on Geodynamics, pp. 55–65. Sci. Rep. No. 14.

Noller, J., Wells, L., Reinhart, E., Rothaus, R., 1997. Subsidence of the harbor at Kenchreai, Saronic Gulf, Greece, during the earthquakes of AD 400 and AD 1928 (Fall meeting abstract). In: EOS (Ed.), Transactions American Geophysical Union 78.

Okada, Y., 1992. Internal deformation due to shear and tensile faults in a half-space. Bull. Seismol. Soc. Am. 82, 1018–1040.

Pantosti, D., Collier, R., D'Addezio, G., Masana, E., Sakellariou, D., 1996. Direct geological evidence for prior earthquakes on the 1981 Corinth fault (central Greece). Geophys. Res. Lett. 22, 3795–3798.

Papazachos, B.C., Papazachou, C.B., 1997. The Earthquakes of Greece. Ziti Editions, Thessaloniki.

Proffett, J.M., 1977. Cenozoic geology of the Yerington district, Nevada, and implications for the nature and origin of Basin and Range faulting. Geol. Soc. Am. Bull. 88, 247–266.

Rothaus, R., Reinhardt, E.G., Noller, J.S., 2008. Earthquakes and subsidence at Kenchreai: using recent earthquakes to reconsider the archaeological and literary evidence. In: Caraher, W.R., Hall, L.J., Moore, R.S. (Eds.), Archaeology and History in Medieval and Post-Medieval Greece: Studies on Method and Meaning in Honor of Timothy E. Gregory. Ashgate.

Scholz, C.H., Contreras, J.C., 1998. Mechanics of continental rift architecture. Geology 26, 967–970.

Scranton, R.L., Ramage, E.S., 1967. Investigations at Corinthian Kenchreai. Hesperia 36, 124–186.

Sibson, R.H., 1977. Fault rocks and fault mechanisms. J. Geol. Soc. Lond. 133, 191–213.

Slemmons, D.B., 1957. Geological effects of the Dixie Valley-Fairview Peak, Nevada, earthquakes of December 16, 1954. Bull. Seismol. Soc. Am. 47, 353–375.

Staley, D.M., Wasklewicz, T.A., Blaszczynski, J.S., 2006. Surficial patterns of debris flow deposition on alluvial fans in Death Valley, CA using airbourne laser swath mapping data. Geomorphology 74, 152–163.

Talebian, M., Biggs, J., Bolourchi, M., Copley, A., Ghassemi, A., Ghorashi, M., Hollingsworth, J., Jackson, J., Nissen, E., Oveisi, B., Parsons, B., Priestley, K., Saiidi, A., 2006. The Dahuiyeh (Zarand) earthquake of 2005 February 22 in central Iran: reactivation of an intramountain reverse fault. Geophys. J. Int. 164, 137–148.

Westoby, M.J., Brasington, J., Glasser, N.F., Hambrey, M.J., Reynolds, J.M., 2012. 'Structure-from-motion' photogrammetry: a low-cost, effective tool for geoscience applications. Geomorphology 179, 300–314. https://doi.org/10.1016/j.geomorph.2012.08.021.

Whipple, K.X., Dunne, T., 1992. The influence of debris-flow rheology on fan morphology, Owens Valley, California. Geol. Soc. Am. Bull. 104, 887–900.

Yamasaki, T., Wright, T.J., Houseman, G.A., 2014. Weak ductile shear zone beneath a major strike-slip fault: inferences from earthquake cycle model constrained by geodetic observations of the western North Anatolian Fault Zone. J. Geophys. Res. 119. https://doi.org/10.1002/2013JB010347.